Journal of the European Ceramic Society 21 (2001) 659–668

www.elsevier.com/locate/jeurceramsoc

Fabrication and characterisation of $La_{0.8}Sr_{0.2}MnO_3$/metal interfaces for application in SOFCs

J.Q. Li, P. Xiao *

Department of Materials Engineering, Brunel University, Uxbridge UB8 3PH, UK

Received 30 March 2000; received in revised form 27 July 2000; accepted 31 July 2000

Abstract

Fabrication and characterisation of $La_{0.8}Sr_{0.2}MnO_3$ (LSMO)/metal interfaces are important for the application of LSMO as the cathode and the metal as the interconnector in solid oxide fuel cells (SOFCs). Interfaces between LSMO and either Fecralloy, or Cr–5Fe–Y_2O_3, or Pt metal were fabricated by using screen printing, followed by sintering at 1200°C in different atmospheres. The microstructures of these LSMO/metal interfaces were examined using scanning electron microscopy (SEM) coupled with energy dispersive spectroscopy (EDS) and X-ray diffraction analysis. The electrical properties were characterised using impedance spectroscopy. The LSMO/Fecralloy interface fabricated in air shows a high electrical resistance (about 10^5 Ω cm^2 at 800°C) due to the formation of an interlayer consisting of alumina and the mixed oxide $M_2O_3{\cdot}nAl_2O_3$ at the interface during the fabrication process. When the interface was fabricated at 1200°C in argon or vacuum, a thicker interfacial layer was formed compared with that formed in air. In addition, the $La_{0.8}Sr_{0.2}MnO_3$ decomposed into $(La_{0.8}Sr_{0.2})_2MnO_{4+\lambda}$, $(La, Sr)_2O_3$ and MnO. Annealing of the specimen at 1200°C for 5 h in air can partially reverse the decomposition. The interface resistance of the annealed sample across the interface is one order of magnitude lower than that of an interface fabricated in air. A thick Cr_2O_3 layer was found at the LSMO/Cr–5Fe–Y_2O_3 interface fabricated in air and a spinel phase $(Mn, Cr)_3O_4$ formed a network surrounding LSMO grains due to the reaction between LSMO phase and CrO_3 vapour released from the Cr_2O_3 layer during the fabrication. The electrical resistances of both phases are high at room temperature, but become significantly lower at 400°C. They can be negligible above 500°C. However the evaporation of CrO_3 increases the resistivity of the LSMO layer. No reaction or oxidation interlayer was found between LSMO and Pt metal producing an interface resistance of 0.52 Ω cm^2 at room temperature.

Keywords: Electrical properties; Fuel cells; Impedance spectroscopy; Interfaces; $(La,Sr)MnO_3$; Metal; Perovskites

1. Introduction

Solid oxide fuel cells (SOFCs) are electrochemical power sources that directly convert the energy of a chemical reaction into electrical energy with high efficiencies.[1] They have the potential for an environment friendly supply of energy. SOFCs typically consist of electrolyte, cathode, anode and interconnector. In SOFC stacks, individual cells are connected by electrical conducting interconnectors. Yittria stablised zirconia (YSZ) has been normally used as the electrolyte requiring an operating temperature of 800∼1000°C. Considering the chemical stability, thermal expansion match and electrical conductivity, at present, Sr-doped lanthanum manganite (e.g. Sr-doped $LaMnO_3$) is most commonly used as cathodes in SOFCs.[2] YSZ/Ni composites are normally used as anodes. The ceramic $LaCrO_3$ doped with CaO or SrO is normally used as the interconnector.[1]

The use of a metallic interconnector rather than a $LaCrO_3$-based ceramic material has the advantage of a higher electronic conductivity, higher ductility, higher heat conductivity and better workability. There have been a few reports on the search for potential metallic alloys as the interconnector.[3–7] Since the interconnector in SOFC is exposed to both air and reducing atmosphere at high temperature (about 1000°C), it is required to have high resistance against high temperature corrosion. To reduce thermal mismatch between different components in SOFCs, the interconnector should also have a coefficient of thermal expansion (CTE) close to those of the electrolyte (YSZ, 11×10^{-6}; see Ref. 6) and cathode (Sr-doped $LaMnO_3$ (LSMO),

* Corresponding author. Fax: +44-1895-812636.
E-mail address: ping.xiao@brunel.ac.uk (P. Xiao).

0955-2219/01/$ - see front matter
PII: S0955-2219(00)00242-9

12×10^{-6}; see Ref. 8). A few studies have been carried out to investigate the possibility of using Cr-containing alloys as interconnectors in SOFCs.[6,7] These have been focused on studying the oxidation resistance and microstructures of the Cr containing alloy/LSMO interfaces. However, little research has been done to investigate the electrical properties of the interface in relation to its microstructure, which is important for application of the alloys as interconnectors and the LSMO as cathodes in SOFCs. In this work, we fabricated interfaces between $La_{0.8}Sr_{0.2}MnO_3$ and either Fecralloy (Fe–22Cr–4.8Al–0.3Si–0.3Y in wt.%), or Cr–5Fe–$1Y_2O_3$ (in wt.%) alloy or Pt metal by screen printing and sintering at 1200°C for 2 h in air. The electrical properties of the different interfaces have been examined using impedance spectroscopy. The effects of interfacial microstructure on the electrical properties of the interfaces have been investigated.

2. Experimental

Three types of metallic materials were used to fabricate LSMO/metal interfaces: Fecralloy (Fe–22Cr–4.8Al–0.3Si–0.3Y in wt.%), chromium base alloy (Cr–5Fe–$1Y_2O_3$ in wt.%) and Pt metal. Fecralloy foils with the thickness of 1.0 mm were obtained from Goodfellow Ltd, UK. The Pt thick film (about 10 μm) was produced on CSZ by using screen printing and sintering. The Cr–5Fe–$1Y_2O_3$ alloy with composition of Cr–5Fe–$1Y_2O_3$ (in wt.%) was prepared using a melting technique. The Sr-doped lanthanum manganite, $La_{0.8}Sr_{0.2}MnO_3$ powder (99.9%, 2 μm), was supplied by Pi Kem Ltd, UK.

Both the Fecralloy and the chromium based alloy were polished using 1200-grit SiC paper to remove the oxide layer at the surface. Then they were ultrasonically cleaned in acetone. The LSMO powder was mixed with Blythe binder (John Mathew Ltd, UK) containing 50% solvent terpineol and 50% ethyl cellulose to make a paste. The paste was then screen printed onto either the Feralloy foil, or the Cr–Fe alloy foil or Pt thick film to form a layer with thickness of about 60∼80 μm. The sample was initially dried at 120°C for 6 h in air. Finally, it was heated upto 1200°C in air, argon or vacuum of 5×10^{-5} torr at a heating rate of 5°C/min and held for 2 h before cooling down to room temperature at the same rate. Some samples were post annealed at 1200°C in air for a certain period to study the interface stability.

A cross-section of the samples was examined using a scanning electron microscope (SEM) coupled with EDX (Jeol JXA-840). The phases present in the thick film layer were identified using X-ray diffraction analysis (Phillips PW 1140). AC impedance of the LSMO/metal interfaces was measured using a computer-controlled Solartron SI 1255 Hf Frequency response/1296 dielectric Interface Analyser over the frequency range of 10^6–10^{-3} Hz. The sample was kept at the measurement temperature for an half hour before impedance measurements were taken. The Zview Impedance Analysis Software was used to analyse the impedance spectra. The metal side of the sample were polished using 1200 grit SiC paper to remove the oxide layer formed during fabrication and then cleaned with acetone. Pt foils were used as electrodes for impedance measurements as shown in Fig. 1. The contact resistance between the Pt and the surface of samples was found to be negligible.

3. Results and discussion

3.1. Interface between $La_{0.8}Sr_{0.2}MnO_3$ and Fecralloy

Fig. 2(a) shows a SEM micrograph of a cross-section of the LSMO/Fecralloy sample fabricated at 1200°C in air. Although a strong bond was achieved between LSMO and Fecralloy, an oxide layer of about 3.0 μm thickness was formed at the interface. Microanalysis indicated that a part of the oxide layer close to the Fecralloy substrate was high purity Al_2O_3 while the other part close to the LSMO contains a second phase in the Al_2O_3 matrix. The second phase was identified as mixed oxide $M_2O_3{\cdot}nAl_2O_3$ where M is mainly La and Sr, together with some Mn. No evidence was found to show that any element from the Fecralloy diffuses into LSMO. X-ray diffraction analysis of the LSMO shows that only the single conducting phase $La_{0.8}Sr_{0.2}MnO_3$ exists in the LSMO layer [see Fig. 3(a)], but the interface resistance of the sample was found to be very high due to the formation of the alumina layer in the interface.

We tried to reduce the thickness of the interfacial oxide layer by fabricating the samples in flowing Ar or vacuum. Fig. 2(b) and (c) show SEM micrographs of the cross-section of LSMO/Fecralloy interfaces fabricated in flowing Ar and vacuum respectively. The microstructures of these two samples at the interfaces are very similar. It is surprising to find that the oxide layers at the interfaces of these two samples are much thicker than that formed in air. The thicker oxide layer is mainly Al_2O_3 phase together with some $M_2O_3{\cdot}nAl_2O_3$ phase (white region). Moreover, the LSMO phase was found to decompose completely into three phases, a light grey phase, a dark grey phase and a white phase during the sintering process. The EDS and X-ray diffraction [Fig. 3(b) and (c)] analysis of the LSMO indicated that the light grey phase, dark grey phase and white phase are $(La_{0.8}Sr_{0.2})_2MnO_{4+\lambda}$, MnO and $(La,Sr)_2O_3$ (the solution of Sr in La_2O_3) phases, respectively. The light grey layer formed on the oxide layer is $(La_{0.8}Sr_{0.2})_2MnO_{4+\lambda}$ phase, next to dark grey (MnO) layer. According to the phase diagram of the La–Sr–Mn–O system,[9] the compound $(La_{0.8}Sr_{0.2})MnO_3$

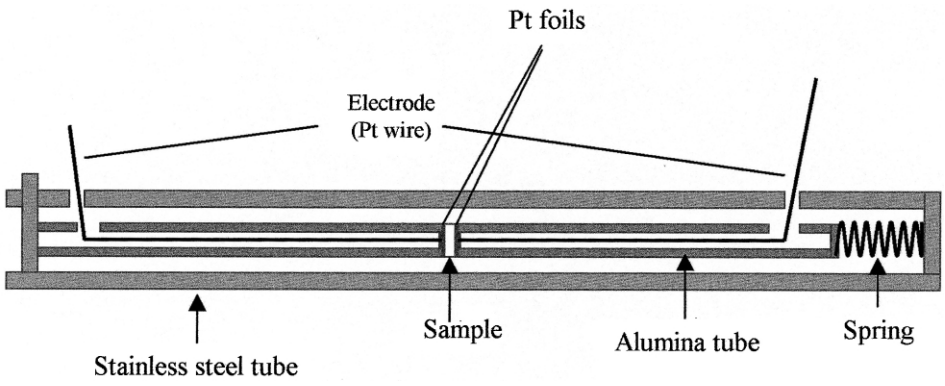

Fig. 1. Sample holder for impedance measurements at high temperature.

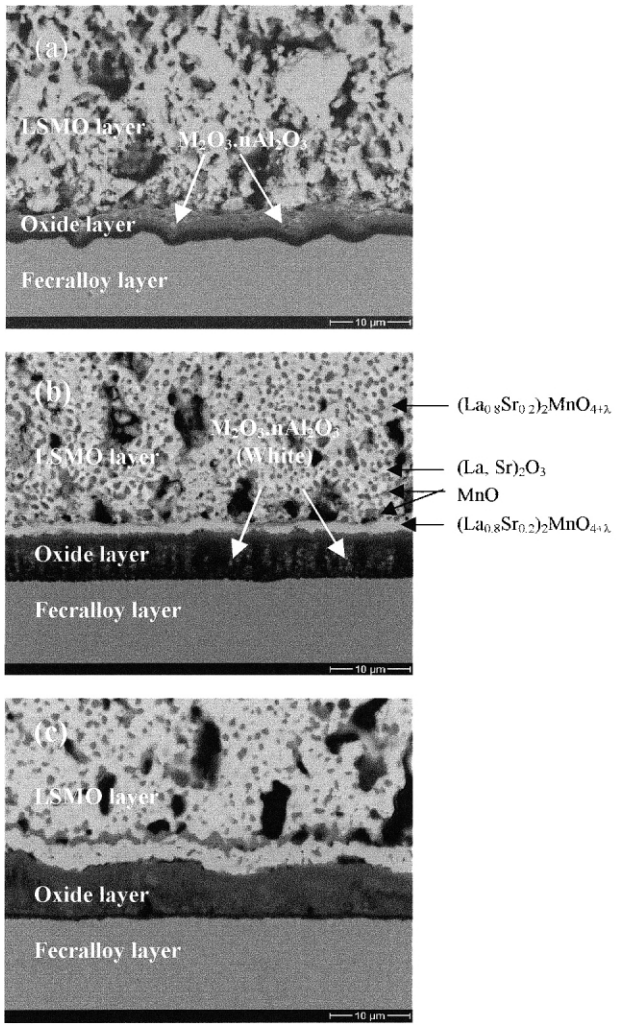

Fig. 2. SEM micrographs of a cross-section of the LSMO/Fecralloy interface fabricated at 1200°C for 2 h in (a) air, (b) flowing Ar and (c) vacuum; the phases in the LSMO layer in (b) and (c) are $(La_{0.8}Sr_{0.2})_2MnO_{4+\lambda}$ (light grey region), $(La, Sr)_2O_3$ (white region) and MnO (dark grey region).

decomposes into $(La_{0.8}Sr_{0.2})_2MnO_{4+\lambda}$, $(La, Sr)_2O_3$ and MnO oxides at 1100°C with an equilibrium oxygen pressure of $Po_2 = 10^{-13}$ atm (10^{-8} Pa). In this work, the oxygen pressure in the vacuum furnace is about 10^{-4} Pa and even higher in the flowing Ar furnace. However, it is expected that the oxygen pressure at the interface of the samples is significantly lower than the oxygen pressure in the furnace chamber.

Experiments showed that there was no decomposition of the $(La_{0.8}Sr_{0.2})MnO_3$ when a pure ceramic specimen was treated using the same thermal process used for the fabrication of the LSMO/Fecralloy interface. Therefore, the LSMO/Fecralloy interfacial reaction promotes the diffusion of oxygen from the LSMO to react with the alloy forming alumina. The decomposition of the $(La_{0.8}Sr_{0.2})MnO_3$ phase leads to poor electrical conductivity in the LSMO thick film layer. However, the decomposition can be partially reversed after thermal treatment of the LSMO/Fecralloy interface at 1200°C for 5 h in air [Fig. 4(a) and (b)] when the LSMO thick film becomes very conductive.

Impedance spectroscopy was used to determine the electrical resistance of the LSMO/Fecralloy interfaces. The sample fabricated in air at 1200°C for 2 h (Air 2), and the sample fabricated in flowing Ar at 1200°C for 2 h followed by thermal treatment in air at 1200°C for 5 h (Ar 2 + Air 5) were used for this impedance measurement. Fig. 5 shows impedance plots of these two samples measured at 600°C. Only one semicircle appears in the complex impedance spectra. Since the LSMO thick film layer and alloy substrate are electric conductors, the semicircle corresponds to the oxide layer formed at the interface in the specimens. Fig. 6 shows the equivalent circuit used for fitting the impedance spectra of the specimens, where R_1 is the resistance of the LSMO thick film layer since the alloy substrate resistance is negligible, R_2 and C_2 are the resistance and capacitance of the oxide layer at the interface. The values of R_1, R_2 and

C_2, given in Table 1, were obtained by simulating the complex impedance spectra using Zview Impedance Analysis Software. Considering the oxide layer at the interface as the dielectric material of a parallel-plane capacitor, the capacitance can be calculated as

$$C = \frac{\varepsilon\varepsilon_0 S}{d}$$

where ε is the dielectric constant of the oxide, ε_0 is the permitivity of vacuum, S is the area of the plane and d is the distance between the two planes (the thickness of the oxide layer in interface). As the capacitance is inversely proportional to the thickness of the oxide layer d and assuming that dielectric constants of oxide layers in both specimens are similar, the ratio between the thickness of the oxide layer formed in Ar and that in air is

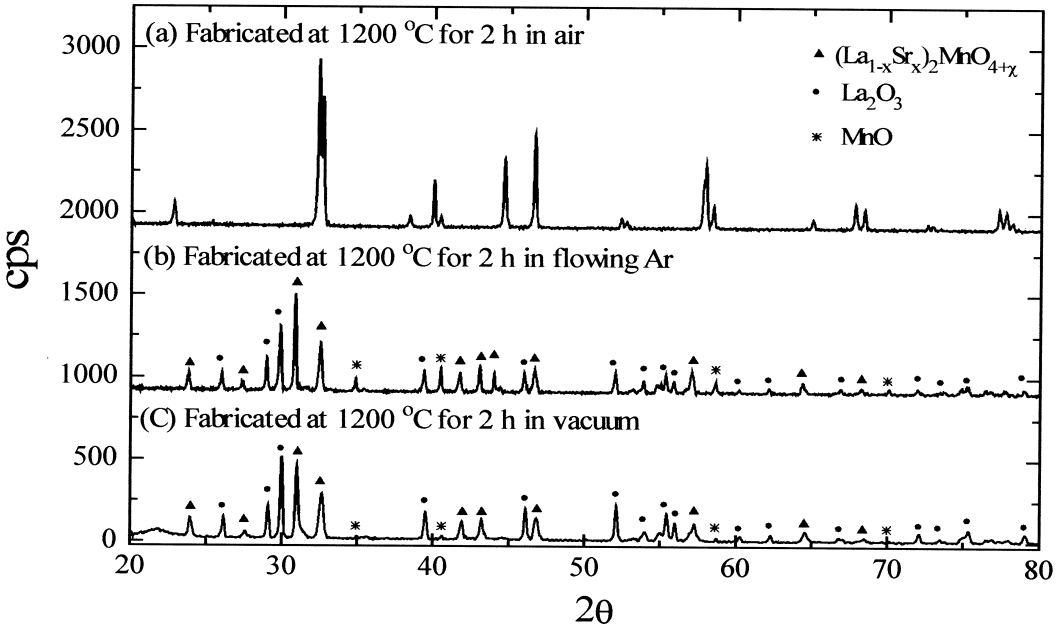

Fig. 3. X-ray diffraction patterns from the surface of LSMO thick film of a LSMO/Fecralloy sample fabricated at 1200°C for 2 h in (a) air, (b) flowing Ar and (c) vacuum.

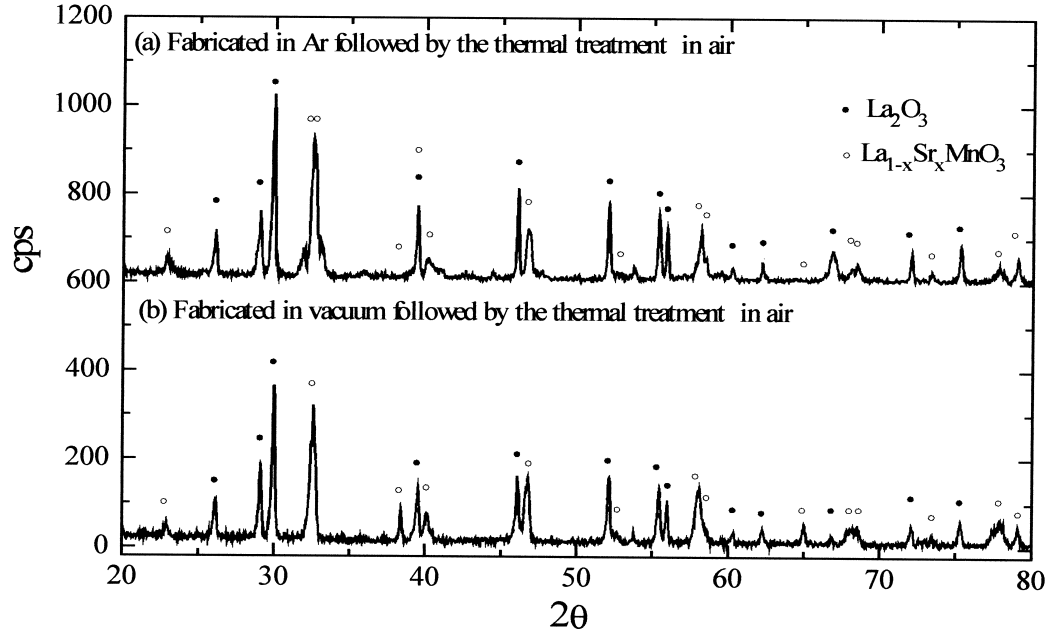

Fig. 4. X-ray diffraction analysis of LSMO in the LSMO/Fecralloy sample fabricated at 1200°C for 2 h in (a) flowing Ar and (b) vacuum followed by thermal treatment at 1200°C in air for 5 h.

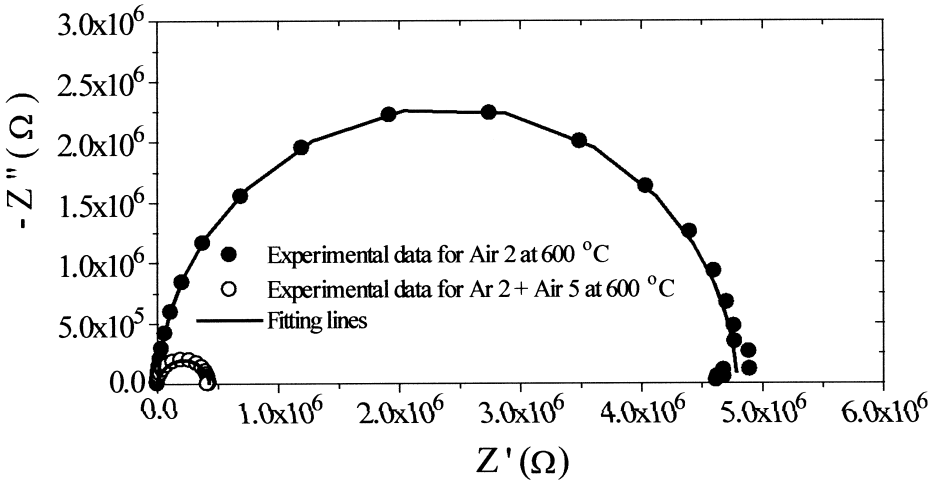

Fig. 5. Impedance diagrams of the LSMO/Fecralloy sample either fabricated in air; or fabricated in flowing Ar followed by thermal treatment at 1200°C in air for 5 h.

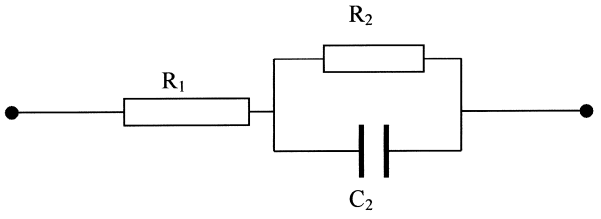

Fig. 6. Equivalent circuit representing the LSMO/Fecralloy interface; R_2 and C_2 represent the resistance and capacitance of the oxide layer; R_1 represents the resistance of the LSMO layer.

calculated as 1.44–1.61 (Table 1). The observation of the oxide layers using SEM show that the thickness of the oxide in the sample fabricated in air is 3 μm whereas the thickness of the oxide fabricated in Ar is 5.5 μm, therefore, the ratio is 1.83. This is close to the results from impedance measurements.

However, the electrical resistance of the interface in the sample fabricated in flowing Ar followed by the thermal treatment in air is about one magnitude lower than that for the sample fabricated in air (see Fig. 5). Fig. 7 shows the resistivity of the oxide layer calculated from its resistance for the two samples and the resistivity of pure polycrystalline Al_2O_3 obtained from Ref. 10. By fitting the plots in Fig. 7, the electrical resistivity of both samples can be expressed as

$$\rho_2^{\text{air}} = 3.65 \times 10^6 e^{0.62(\text{eV})/KT} (\Omega\,\text{cm})$$

$$\rho_2^{\text{Ar}} = 4.51 \times 10^5 e^{0.60(\text{eV})/KT} (\Omega\,\text{cm})$$

respectively. Although the resistivity of the oxide layers is lower than that of the pure alumina, the interface electrical resistance is still too high to be used as interconnector in SOFCs.

3.2. Interface between $(La_{0.8}Sr_{0.2})MnO_3$ and Cr-5Fe-1Y_2O_3 alloy

Fig. 8 shows a SEM micrograph of a cross-section of the interface between $(La_{0.8}Sr_{0.2})MnO_3$ and the Cr–5Fe–Y_2O_3 alloy. A good bond at this interface can be obtained by using our fabrication methods. A thick oxide layer (about 10 μm) was formed at the interface during fabrication. EDX analysis indicated that this oxide layer was a high purity Cr_2O_3 phase [see Fig. 9(a)]. Cr cannot be detected within the LSMO grains [Fig. 9(b)], but Cr and Mn are enriched in the grey

Table 1
The resistance of LSMO layer (R_1), the resistance and capacitance of oxide layer (R_2, C_2) formed between LSMO and metal[a]

Temperature (°C)	Air 2			Ar 2 + Air 5			$C_{2,air2}/C_{2,Ar2+Air5}$
	R_1 (Ω cm^2)	R_2 (Ω cm^2)	C_2 (F)	C_2 (F)	R_1 (Ω cm^2)	R_2 (Ω cm^2)	
200	7.5	3.15×10^{9}	9.2×10^{-9}	1.48×10^{-8}	18.0	3.16×10^{8}	1.61
400	6.5	5.71×10^{7}	1.12×10^{-8}	1.69×10^{-8}	15.0	6.88×10^{6}	1.51
600	5	4.70×10^{6}	1.32×10^{-8}	1.90×10^{-8}	9.0	4.28×10^{5}	1.44
800	3	6.00×10^{5}	1.68×10^{-8}	2.60×10^{-8}	7.0	7.58×10^{4}	1.55

[a] The oxide layer was formed either during fabrication in air (Air 2) or fabrication in flowing Ar followed by thermal treatment at 1200°C in air (Ar 2 + Air 5).

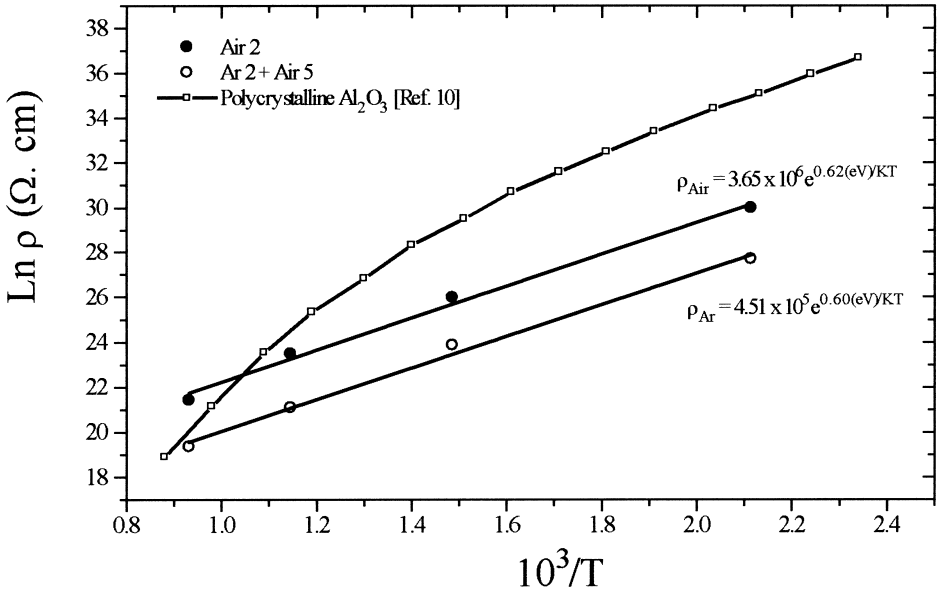

Fig. 7. Ln R_2 (the resistance of oxide layer at the interface) vs $10^3/T$ for the LSMO/Fecralloy sample (a) fabricated in air and (b) fabricated in flowing Ar followed by thermal treatment at 1200°C for 5 h in air.

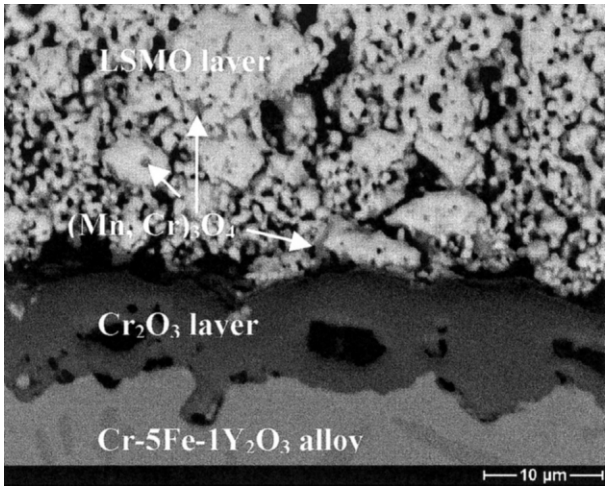

Fig. 8. SEM micrographs of a cross-section of the LSMO/Cr–5Fe–1Y_2O_3 interface fabricated at 1200°C for 2 h in air.

regions of the cross-section (Fig. 8). The grey regions were not only present near the interface, but also within the LSMO thick film layer [Fig. 9(c) and (d)]. The formation of this grey phase is due to the reaction between the LSMO phase and CrO_3 vapour released from the Cr_2O_3 oxide layer at the interface at high temperature. X-ray diffraction analysis of the surface of LSMO/Cr–5Fe–Y_2O_3 specimen after post annealing at 1200°C for 10 h suggests that this grey phase is a spinel phase (Mn, Cr)$_3O_4$ (Fig. 10). This spinel phase is present in pores and voids of the LSMO layer and seems to form a network surrounding LSMO grains.

Fig. 11 shows a typical impedance plot of the as-prepared LSMO/Cr–5Fe–1Y_2O_3 interface. There are two depressed semicircles in the complex impedance spectrum, which corresponds to the Cr_2O_3 layer at the interface and the (Mn, Cr)$_3O_4$ network in the LSMO thick film layer. To simulate the electrical behaviour of these oxides, two parallel R-CPE (constant phase element) equivalent circuits in series are assumed (Fig. 12), where R_1 is the resistance of the LSMO thick film layer, R_2 and R_3 are the resistances of and CPE_2 and CPE_3 are capacitance of Cr_2O_3 and (Mn, Cr)$_3O_4$ as functions of frequency. The constant phase elements (CPEs) are used in the equivalent circuit because the semicircles in the spectra are significantly depressed, indicating that the oxide layer is not single phase with a single relaxation frequency. The CPE is used here in place of a capacitor to represent the non-homogeneous materials. The impedance of the CPE is $Z = 1/[T(i\omega)^P]$, where T and P are two parameters, ω is the angular frequency of AC signal and $i = \sqrt{-1}$. When $P = 1$, the equation represents the impedance of a capacitor. The deviation of P from 1 corresponds to porosity and non-homegeneity of the materials determined. For the LSMO/Cr–5Fe–1Y_2O_3 interface, due to the porous nature and network distribution of (Mn,Cr)$_3O_4$ phase, we assume that the parameter P for the simulation of the (Mn, Cr)$_3O_4$ phase is smaller than that of the Cr_2O_3 layer. Based on simulation of the impedance spectra in Fig. 11, the parameter P for simulation of the first semicircle (at high frequency) is about 0.9~1 whereas the P value for the second semicircle (at low frequency) is around 0.7. Therefore, it is likely that the Cr_2O_3 layer corresponds to the first semicircle whereas the (Mn, Cr)$_3O_4$ phase corresponds to the second semicircle. Therefore, the resistor R_2 corresponds to Cr_2O_3 layer, and R_3 corresponds to the (Mn, Cr)$_3O_4$ phase. The electrical resistances, R_2 and R_3, obtained by simulating the complex

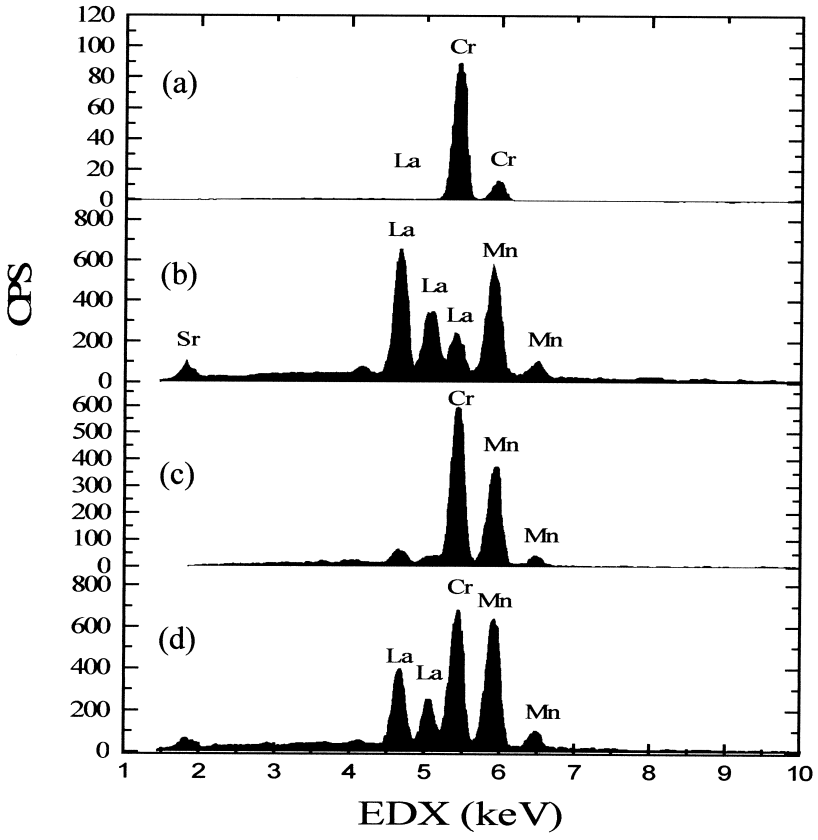

Fig. 9. EDX analysis of (a) the interlayer at the interface, (b) LSMO grain (white region in LSMO thick film region), (c) the grey region near the interlayer in LSMO thick film region and (d) the grey region far from the interlayer in LSMO thick film region for the LSMO/Cr–5Fe–1Y_2O_3 specimen.

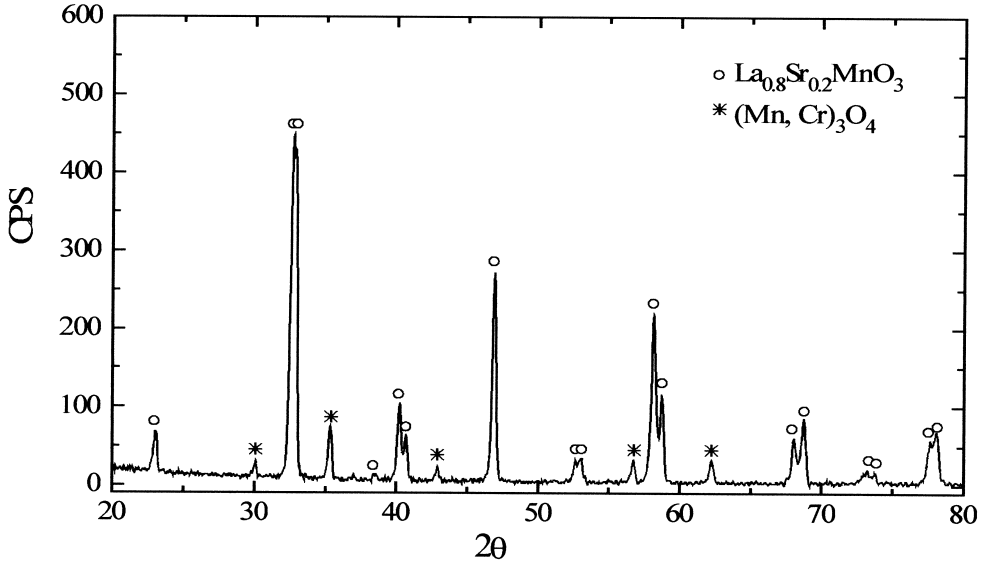

Fig. 10. X-ray diffraction analysis of the LSMO phase in the LSMO/Cr–5Fe–1Y_2O_3 sample fabricated at 1200°C for 2 h in air followed by thermal treatment in air at 1200°C for 10 h.

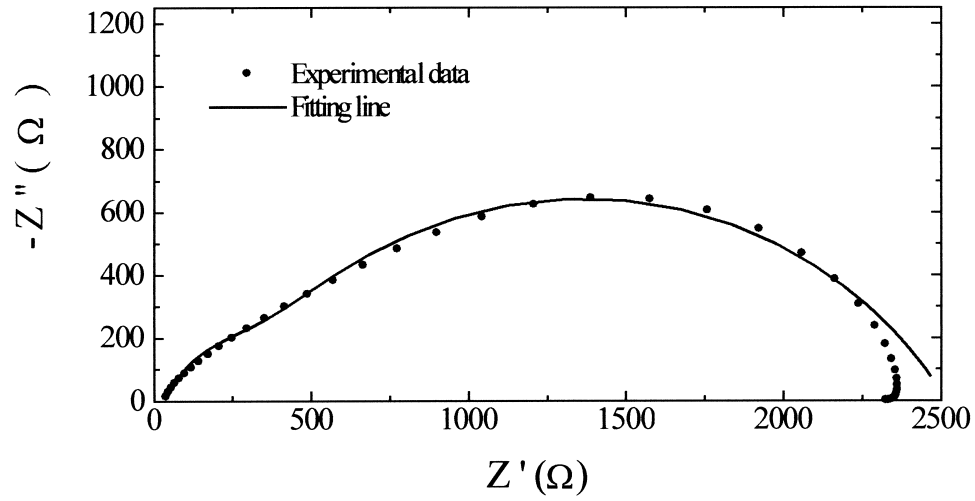

Fig. 11. Impedance diagram of the as-prepared LSMO/Cr–5Fe–1Y_2O_3 interface measured at 200°C.

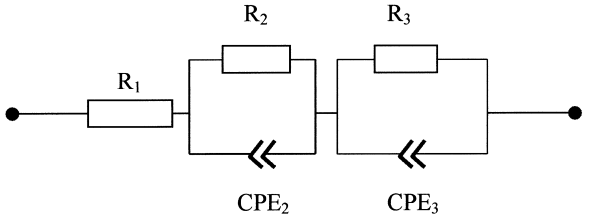

Fig. 12. Equivalent circuit representating the LSMO/Cr–5Fe–1Y_2O_3 interface; R_2 and CPE_2 represent the resistance and capacitance effect of the Cr_2O_3 layer; R_3 and CPE_3 represent the resistance and capacitance effect of the $(Mn,Cr)_3O_4$ spinel phase; and R_1 represents the resistance of the LSMO layer.

impedance spectra for the two phases, are high at room temperature [3.62×10^4 and 1.87×10^5 Ω cm^2 for the Cr_2O_3 oxide layer and the $(Mn, Cr)_3O_4$ network, respectively], but become significantly lower at 400°C (1.7 and 7.4 Ω cm^2, respectively). They are negligible at temperature above 500°C. Fig. 13 shows the R_2 and R_3 as a function of temperature. The resistivity of pure Cr_2O_3 crystal (solid line) and Mn_3O_4 (dash line) obtained from Ref. 11 are also shown in Fig. 13. The $\ln(R)$ vs. $10^3/T$ for these two phases in our work do not show linear relationships due to the porosity and impurities in these two phases. The sample after thermal

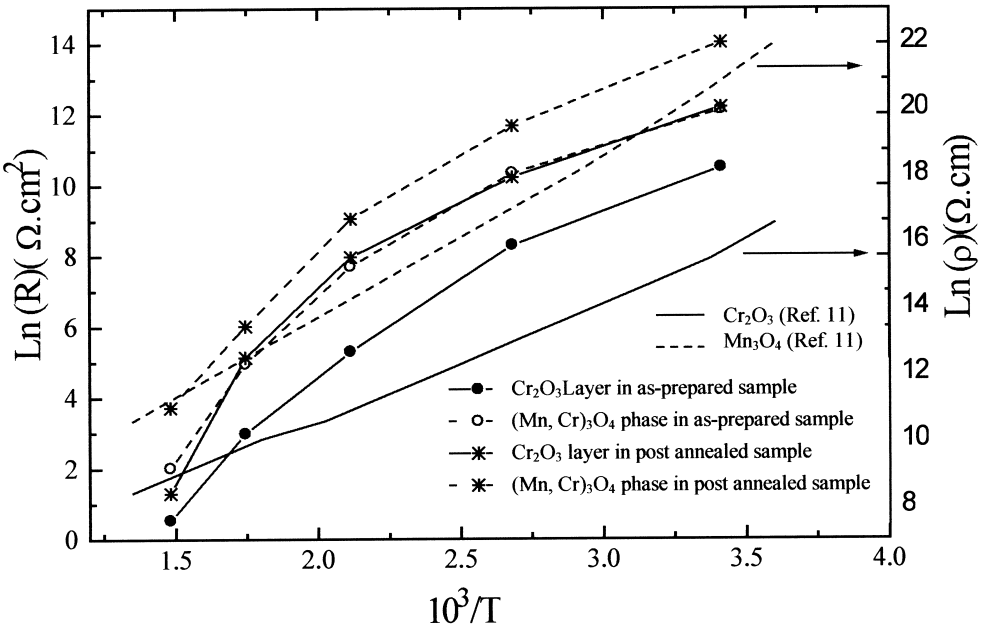

Fig. 13. Ln R_2 (resistance of Cr_2O_3 layer), ln R_3 [resistance of $(Mn,Cr)_3O_4$ spinel phase] vs $10^3/T$ for as-prepared and subsequent thermally treated LSMO/Cr–5Fe–1Y_2O_3 interfaces.

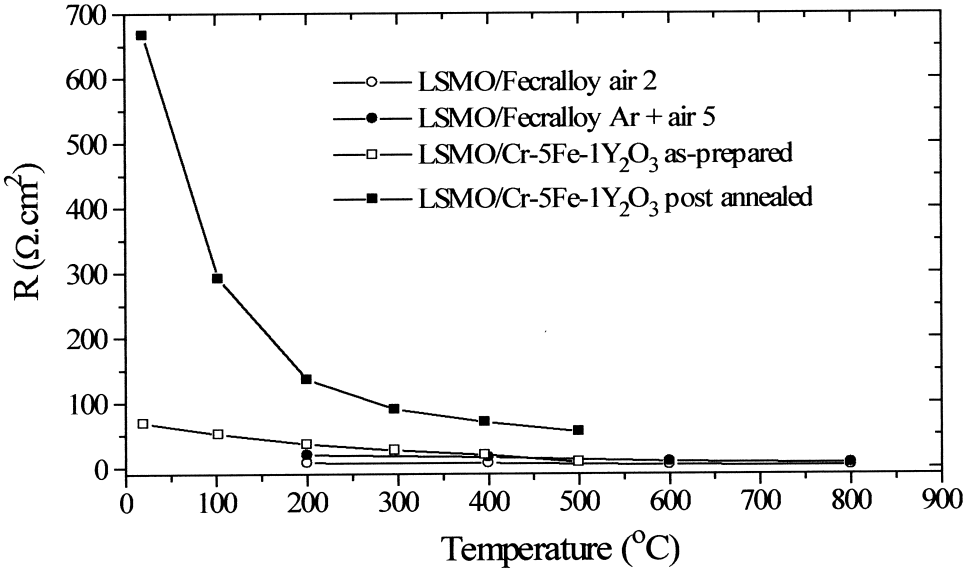

Fig. 14. Resistance of the LSMO layer in the LSMO/Fecralloy and LSMO/Cr–5Fe–$1Y_2O_3$ interfaces as function of temperature.

treatment at 1200°C for 5 h in air also shows similar complex AC impedance spectra with higher resistance due to the growth of Cr_2O_3 layer at the interface and the $(Mn, Cr)_3O_4$ network in LSMO thick film layer. However, the resistance becomes significantly lower above 450°C.

Fig. 14 shows the resistance of the LSMO layer (R_1 in Figs. 6 and 12) in the LSMO/Fecralloy and LSMO/Cr–5Fe–$1Y_2O_3$ interface. In the first interface, the resistances of LSMO are small for the specimens fabricated both in air and Ar with thermal treatment afterwards. In the second interface, the resistance of the LSMO layer was small after fabrication, but increased significantly after thermal treatment in air at 1200°C for 10 h (660 Ω cm^2 at room temperature and 55.0 Ω cm^2 at 500°C). This phenomenon may be caused by evaporation of CrO_3 into the LSMO layer. This indicates that the main disadvantage of the LSMO/Fe–5Cr–$1Y_2O_3$ interface for application in SOFCs is degradation of the LSMO phase due to reaction with CrO_3 vapour.

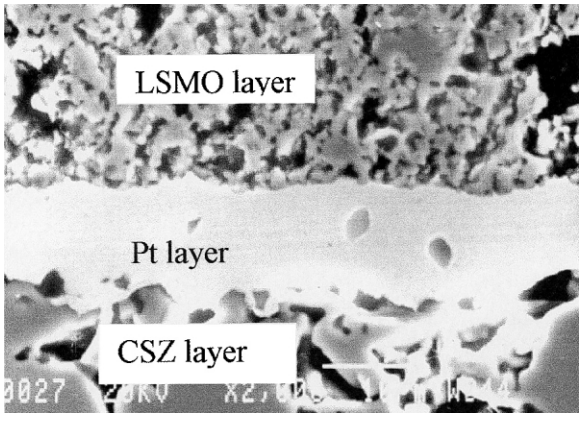

Fig. 15. SEM micrograph of cross-section of the LSMO/Pt interface.

3.3. Interface between $(La_{0.8}Sr_{0.2})MnO_3$ and Pt metal

A LSMO/Pt interface was fabricated by using screen printing of LSMO on Pt and then sintering the specimen at 1200°C for 2 h in air. Fig. 15 shows the SEM micrograph of this interface where no reaction layer is found. The interface electrical resistance measured using a multimeter is 0.52 Ω cm^2 at room temperature. Thermal treatment at 1200°C caused no change in the electrical resistance of the interface.

4. Conclusion

We have fabricated LSMO/Fecralloy, LSMO/Cr–5Fe–$1Y_2O_3$ and LSMO/Pt interfaces and examined their microstructures and interface electrical resistances. Experimental results show that the resistance of the LSMO/Fecralloy interface is very high due to the presence of electrical insulating oxide layer consisting of Al_2O_3 and $M_2O_3{\cdot}nAl_2O_3$ phases, which were formed at the interface during fabrication. The LSMO/Cr–5Fe–$1Y_2O_3$ interface shows low an electrical resistance although both Cr_2O_3 and $(Mn, Cr)_3O_4$ phases were formed during fabrication. However, the reaction between CrO_3 vapour and the LSMO phase increases the resistivity of the LSMO layer. A LSMO/Pt interface shows good bonding and low resistance, which is suitable for application of SOFCs. Coating Pt on Cr–5Fe–$1Y_2O_3$ alloy before bonding to the LSMO may prevent the evaporation of CrO_3 phase at the service temperature for application of LSMO/Cr–5Fe–$1Y_2O_3$ interface in SOFCs.

Acknowledgements

The authors would like to acknowledge Dr. J. Shemilt for useful advice on the preparation of the manuscript. This work is supported by Engineering and Physical Science Research Council (EPSRC, GM/M40271) of the UK.

References

1. Minh, N. Q., Ceramic fuel cells. *J. Am. Ceram. Soc*., 1993, **76**, 563–588.
2. Carter, S., Selcuk, A., Chater, R. J., Kajda, J., Kilner, J. A. and Steele, B. C. H., Oxygen-transport in selected nonstoichiometric perovskite-structure oxides. *Solid State Ionics*, 1992, **53/56**, 597–605.
3. Thierfelder, W., Greiner, H. and Kock, W., High-temperature corrosion behaviour of chromium based alloys for high temperature SOFC. In: *Proceedings of the Fifth International Symposium on Solid Oxide Fuel Cells (SOFC-V)*. Electrochem. Soc., Pennington, NJ, 1997, pp. 1306–1315.
4. Kofstad, P. and Bredesen, R., High temperature corrosion in SOFC environments. *Solid State Ionics*, 1992, **52**, 69–75.
5. Kadowaki, T., Shiomitsu, T., Matsuda, E., Nakagawa, H., Tsuneizumi, H. and Maruyama, T., Applicability of heat resisting alloys to the separator of planar type solid oxide fuel-cell. *Solid State Ionics*, 1993, **67**, 65–69.
6. Linderoth, S., Hendriksen, P. V., Mogensen, M. and Langvad, N., Investigations of metallic alloys for use as interconnects in solid oxide fuel cell stacks. *J. Mater. Sci*., 1996, **31**, 5077–5082.
7. Quadakkers, W. J., Greiner, H., Hansel, M., Pattanaik, A., Khanna, A. S. and Mallener, W., Compatibility of perovskite contact layers between cathode and metallic interconnector plates of SOFCs. *Solid State Ionics*, 1996, **91**, 55–67.
8. Srilomsak, S., Schilling, D. P. and Anderson, H. U., Thermal expansion studies on cathode and interconnect oxide. In *Proceeding of the first International Symposium on Solid State Fuel Cell*, ed. S. C. Singhal. The Electrochemical Society, Pennington, NJ, 1989, pp. 129–240.
9. Cherepanov, V. A., Yu-Barkhatova, L. and Voronin, V. I., Phase equilibria in the La–Sr–Mn–O system. *J. Solid State Chem*., 1997, **134**, 38–44.
10. Kingery, W. D., Bowen, H. K. and Uhlmann, D. R., *Introduction to ceramic*, 2nd edn. John Wiley & Son, Inc., New York, 1976, p. 905.
11. Kingery, W. D., Bowen, H. K. and Uhlmann, D. R., *Introduction to ceramic*, 2nd edn. John Wiley & Son, Inc., New York, 1976, p. 867.